

Assessment of solar photovoltaic potentials on urban noise barriers using street-view imagery



Teng Zhong ^{a,b,c,1}, Kai Zhang ^{a,b,c,1}, Min Chen ^{a,b,c,g,*}, Yijie Wang ^{a,b,c}, Rui Zhu ^d,
Zhixin Zhang ^{a,b,c}, Zixuan Zhou ^{a,b,c}, Zhen Qian ^{a,b,c}, Guonian Lv ^{a,b,c}, Jinyue Yan ^{e,f}

^a Key Laboratory of Virtual Geographic Environment (Ministry of Education of PR China), Nanjing Normal University, Nanjing, 210023, China

^b State Key Laboratory Cultivation Base of Geographical Environment Evolution, Nanjing, 210023, China

^c Jiangsu Center for Collaborative Innovation in Geographical Information Resource Development and Application, Nanjing, 210023, China

^d Senseable City Laboratory, Future Urban Mobility IRG, Singapore-MIT Alliance for Research and Technology, 1 Create Way 09-02 Create Tower, 138062, Singapore

^e School of Business, Society & Engineering, Mälardalen University, Västerås, 72123, Sweden

^f Department of Chemical Engineering, KTH Royal Institute of Technology, Stockholm, 10044, Sweden

^g Jiangsu Provincial Key Laboratory for NSLSCS, School of Mathematical Science, Nanjing Normal University, Nanjing, 210023, China

ARTICLE INFO

Article history:

Received 10 July 2020

Received in revised form

12 October 2020

Accepted 10 December 2020

Available online 15 December 2020

Keywords:

Solar radiation assessment

Photovoltaic noise barrier (PVNB)

Street-view images

Object detection

Machine learning

ABSTRACT

Solar energy captured by solar photovoltaic (PV) systems has great potential to meet the high demand for renewable energy sources in urban areas. A photovoltaic noise barrier (PVNB) system, which integrates a PV system with a noise barrier, is a promising source for harvesting solar energy to overcome the problem of having limited land available for solar panel installations. When estimating the solar PV potential at the city scale, it is difficult to identify sites for installing solar panels. A computational framework is proposed for estimating the solar PV potential of PVNB systems based on both existing and planned noise barrier sites. The proposed computational framework can identify suitable sites for installing photovoltaic panels. A deep learning-based method is used to detect existing noise barrier sites from massive street-view images. The planned noise barrier sites are identified with urban policies. Based on the existing and planned sites of noise barriers in Nanjing, the annual solar PV potentials in 2019 are 29,137 MW h and 113,052 MW h, respectively. The estimation results show that the potential PVNB systems based on the existing and planned noise barrier in 2019 have the potential installed capacity of 14.26 MW and 57.24 MW, with corresponding potential annual power generation of 4662 MW h and 18,088 MW h, respectively.

© 2020 Elsevier Ltd. All rights reserved.

1. Introduction

An accurate assessment of the potential for installing solar photovoltaic (PV) panels in urban areas is essential for implementing sustainable technologies and policy solutions at the city scale [1–3]. At present, approximately 55% of the world's population lives in cities, and cities constitute approximately two-thirds of the global primary energy demand [4]. Global energy assessments indicate that compared with fossil fuels, solar energy is a renewable

energy source that causes less harm to the environment [5]. During the past decade, there has been a 50% increase in global solar PV demand. While centralized solar power plants require large areas for PV system installation, urban areas possess only limited space for solar PV module installation due to the high price of land [6]. Significant efforts have been made to estimate the solar PV potential of rooftop PV systems in which a large number of small-scale solar PV modules are installed on rooftops [7,8]. The density of high-rise cities, however, means that insufficient rooftop space exists to meet the high solar energy demand. In addition, building-integrated PV systems still have many unsolved health, and safety issues remain [6].

Currently, PV system integration with urban noise barriers has attracted considerable attention in many countries [9]. A noise barrier is a common form of construction located near roadways in

* School of Geography, Nanjing Normal University, NO.1 Wenyuan Road, Qixia District, Nanjing 210023, PR China.

E-mail addresses: chenmin0902@njnu.edu.cn, chenmin0902@163.com (M. Chen).

¹ Both authors contributed equally to this study.

urban environments to protect inhabitants from noise pollution. The photovoltaic noise barrier (PVNB) system was developed by combining a PV system with a noise barrier. This combination can serve as an alternative solution to address the problem of limited solar resources in densely populated urban areas with high energy needs [10]. While research on establishing the PVNB system from the perspectives of solar panel selection and PV module configuration exists, few studies have evaluated the solar PV potential of urban noise barriers at the city scale. One problem is that at the city scale, it is difficult to identify the road edges where urban noise barriers currently exist. In addition, it is challenging to obtain planned sites for urban noise barrier installation according to urban plan policies.

Geographic Information Systems (GIS) is widely adopted for comprehensive geographic analysis and achieving human-oriented geographic information presentation [11,12]. Rather than modelling the urban system from an aerial view, emerging methods have adopted street-view images, which enable modelling the physical environments of cities at the street level [13]. Massive numbers of street-view images from online map providers such as Google Maps, Baidu Maps, and Tencent Maps have become new data sources that provide unprecedented survey opportunities [14]. Deep learning and computer vision technologies have been applied to design automatic tools for extracting target objects from street-view images [15]. For example, a single shot multi-box detector (SSD), which is a deep convolutional neural network model used for object detection, can accurately extract tiny objects from street-view images [16]. Thus, a big data approach can be used to identify the locations of noise barriers and use them as a primary indicator for estimating the solar PV potential of urban noise barriers.

The primary objective of this study is to develop a framework for estimating the solar PV potential of noise barriers at the city scale. The city of Nanjing, China is adopted as an example to estimate the solar PV potential of noise barriers in Nanjing. The spatial distribution map of the estimated solar PV potential of noise barriers provides the basis for the implementation of the urban plan policy for future utilization of renewable solar PV energy.

2. Literature review

2.1. Solar energy harvesting with a photovoltaic noise barrier

PVNB is not a new technology [8]. Many studies have considered combining the advantages of solar energy resources with the reduction of road traffic noise pollution using PVNB [9,17]. Noise barriers of different types have different physical properties in terms of surface structure, area, orientation, and slope that can restrict the efficiency with which solar PV modules can harvest solar energy [18]. Several studies have concentrated on analysing the effects of noise barrier structural characteristics on the utilization of solar energy resources at the micro-scale [5,14]. PV noise barriers with bifacial PV modules, which receive solar energy on both sides, are considered the best design for capitalizing on noise barrier use [19]. However, the reflection from bifacial PV modules installed on the PVNB can cause driver distraction on roadways, which prevents it from replacing the mono-facial PV modules in the near future [20].

The existing research on PVNBs has primarily focused on the engineering aspects of solar energy harvesting with PVNBs at the macroscale [21]. An assessment of actual photoelectric conversion efficiency and the economic benefits of PVNB indicated that PVNB has substantial development potential and application prospects [9]. A cost-benefit analysis method was proposed to evaluate the economic benefits of PV noise barriers [6]. Although PVNB installations increase the cost of noise barriers, the integration of

solar PVs with noise barriers introduces long-term ecological benefits [6]. This view was also supported by a case study of PVNB installed along a subway; the study conducted economic and environmental benefit analyses to determine whether the PVNB can generate profits [10]. The PV potential of noise barriers on the United States highway system was estimated based on the ratio of highway mileage to the length of PVNBs; the resulting is further compared with the energy demand of the United States to estimate the economic benefit of PVNBs [10].

Although PVNB technology has considerable deployment potential for solar energy harvesting because more than 60 million km of roadway exists in the world [11], it has not yet been widely deployed worldwide.

2.2. Use GIS and remote sensing technology to estimate solar PV potential

The solar PV potential of a city depends on environmental characteristics such as its geographic location and climatic conditions. A geographic information system (GIS) is an ideal tool for analysing the potential for urban solar PV at large spatial scales [22–24]. Many studies have been conducted by combining remote sensing data and GIS technology to estimate urban solar PV potential [25,26]; however, estimating the potential of urban solar PV mainly solves the problem of identifying surfaces suitable for solar utilization and determining the potential of solar PV on solar utilization surfaces [27]. The GIS analysis function, combined with object-specific image recognition, is used to evaluate the solar PV potential of the solar utilization surface [25]. There are also case studies that assess solar radiation based on a 3D height model of the city using the Solar Analyst plugin in ArcGIS, which considers the available surface slope according to the 3D model and accurately describes the different urban constituent elements and their shadows [28]. The cost of acquiring high-resolution satellite images and LiDAR 3D laser point clouds is relatively high, making it impossible to estimate the urban solar PV potential with these high-price remote sensing data [29]. Some studies have proposed the use of free satellite images combined with open source GIS software to estimate the urban PV potential [30,31]. For example, publicly available geographic building data and aerial images can be analysed using image recognition and machine learning techniques to estimate urban PV potential [32]. Google satellite imagery and Google Street View imagery were integrated to build a 3D model for estimating the urban PV potential of building roofs [33].

2.3. Emerging solar PV potential estimation approach with street-view imagery

Several studies have estimated the urban solar PV potential based on field survey statistics and remote sensing data products [34,35]. For example, Bódis et al. evaluated the solar PV potential in the entire EU with an overlay analysis using the statistical data from the European Habitat Maps and European City Atlases [6]. LiDAR data and area-based modelling methods have also been used to estimate the solar potential of multiform building roofs [36]. However, it is difficult to balance the remote sensing quality and the acquisition cost when estimating urban solar PV potential at large spatial scales. The emergence of public map services, e.g., Google Satellite, Google Street View, and Baidu Street View has made street-level urban images available [37] that can accurately reflect information regarding a city's facade. Such data provide new opportunities for solar energy potential estimation at the city level [14]. Open access street-view images have advantages in terms of broad coverage and low acquisition costs compared with high-accuracy remote sensing images.

City facades have a reduced chance of being obscured by dust or snow, which provides better maintenance conditions for PV modules [38]. As an important part of the urban space facade, PVNB can be applied to both reduce noise and generate power without occupying additional land [10]. Urban morphology is an important factor that affects the distribution of urban solar radiation [39]. Regarding urban canyon geometry, the sky view factor (SVF) is closely related to the spatial variability of solar radiation [13]. Street panoramas and building height models can be combined to analyse seasonal variations in solar radiation in street canyons at the city scale [40]. Carrasco-Hernandez et al. reconstructed the street geometry and calculated the total shortwave radiation for the urban canyon of Manchester in England [41].

The current image classification method used for object detection from street-view images is mainly divided into two categories: one-stage and two-stage methods [42]. The one-stage method directly predicts the locations and categories of objects in the image based on a map calculated as the image passes through the network [43]. They have advantages in terms of fast training and recognition speed but also achieve limited classification accuracy [44]. The two-stage methods classify objects based on a prior detection of candidate positions for objects [43]. While these methods typically achieve better detection performance, their training and recognition speeds are not as fast as those of the one-stage methods [44]. The YOLO v3 model is the state-of-art one-stage object detector. It achieves both relatively high accuracy and has a fast detection speed. YOLO v3 has achieved excellent detection results on standardized data sets such as the PASCAL Visual Object Classes (PASCAL VOC) and Microsoft Common Objects in Context (MS COCO) while significantly improving the detection accuracy compared to previous YOLO versions.

In this paper, efficient workflow for estimating the solar PV potential at the city scale is proposed. A deep learning-based target detection method is used to identify existing urban noise barrier sites from massive numbers of street-view images. Then, planned sites for the urban noise barriers are identified based on urban planning policies; these serve as supplemental sites where PV noise barriers could be installed. Finally, the solar PV potential of the city is estimated based on both the existing and planned urban noise barrier sites.

3. Methodology

3.1. Research framework

In this study, a computational framework is developed for estimating the solar PV potential of urban noise barriers with a focus on suitable site selection for PVNB installations. The integration of PV systems with the existing noise barrier is an attractive solution for new PVNB installations. Besides, the sites planned for the construction of noise barriers are also suitable for installing PVNB systems.

The research process for assessing the power generation of solar PV on urban noise barriers in Nanjing (Fig. 1) involves the following three steps:

The first step is to detect existing noise barrier sites in Nanjing automatically. This objective is implemented based on the Nanjing road network data obtained from OpenStreetMap. The sampling points for collecting the street-view image are generated along with the OSM road network at 20-m intervals. YOLO v3 is applied as the object detector to identify the street-view images containing noise barriers from the massive street-view image dataset. The locations of the identified street-view images are map-matched to the corresponding road edge to determine the sites of existing

noise barriers.

The second step to automatically identify planned sites for noise barriers in Nanjing based on urban policy. According to the specifications for noise barrier placement, road network data, and the vector boundaries of buildings in Nanjing from the Mapbox (<https://www.mapbox.com/>), we obtained the planned sites for noise barriers in Nanjing through buffer analysis.

The third step is to estimate the solar PV potential of both the existing and planned urban noise barriers in Nanjing. Based on the site identified in the previous steps, the existing and planned solar PV potential of noise barriers in Nanjing was calculated using a numerical model combined solar radiation data and the pre-determined noise barrier parameters.

3.2. Experimental data acquisition

The experimental area of this study was obtained for Nanjing, Jiangsu Province, China (Fig. 2). The road network in the study area was obtained from OpenStreetMap using the following HTTP request (<https://www.openstreetmap.org/#map=4/36.96/104.17>) performed by Python scripts. The road network includes road attribute information. The roads in this road network have five types: motorways, trunk roads, primary roads, secondary roads, and tertiary roads. Because noise barriers are installed only at the road edges of motorways (Fig. 2c yellow), and trunk roads (Fig. 2c orange), primary roads, secondary roads, and tertiary roads were not included in this study. The building outline data were supplied by Mapbox (<https://www.mapbox.com/>), a website that provides precise location data and can create customized, personalized maps. The building outline vector data for the study area were also obtained through Python scripts (Fig. 2c brown and black). The data include building locations, heights, and other attributes.

Based on the vector data for the motorway and trunk roads in Nanjing, sampled at 20 m intervals, 130,799 total sampling points were extracted. Street-view images were obtained using a Python script constituting an HTTP URL request form that conformed with the Baidu Street View API for accessing the panoramic static image service. The static street-view images can be retrieved by defining URL parameters such as the image size, horizontal range, latitude, longitude, and horizontal viewing angle. Specifically, we set the size of the street-view image to 500 × 400 pixels and set the horizontal range to 90°. Using these values, four images are sufficient to show a panorama of the surrounding environment. In addition, the Baidu Map API uses azimuth an angle to the true north), but most street layouts have a particular perspective to true north. Because noise barriers are mostly distributed on both sides of the roads, setting the horizontal viewing angle to match the road's forward direction would be helpful in detecting any surrounding noise barriers. Therefore, we further calculated the three main attributes needed to sample specific points: longitude, latitude, and road direction. Using these data, we obtained a set of street-view images corresponding to each sampling point, as shown in Fig. 3. The street-view images at clockwise 90° and 270° viewing angles to the road direction were selected to ensure that the noise barrier positions were consistent with the corresponding sampling point. Meanwhile, because most of Nanjing's motorway and trunk roads are two-way roads, to avoid repeated detections, we considered only street-view images with a 90° viewing angle to the road direction (the right side of the current lane) in the experiment.

3.3. Detecting noise barriers from street-view images automatically using deep learning

In this step, the YOLO v3 object detector, which is based on deep learning algorithms, is used to identify the sites of existing noise

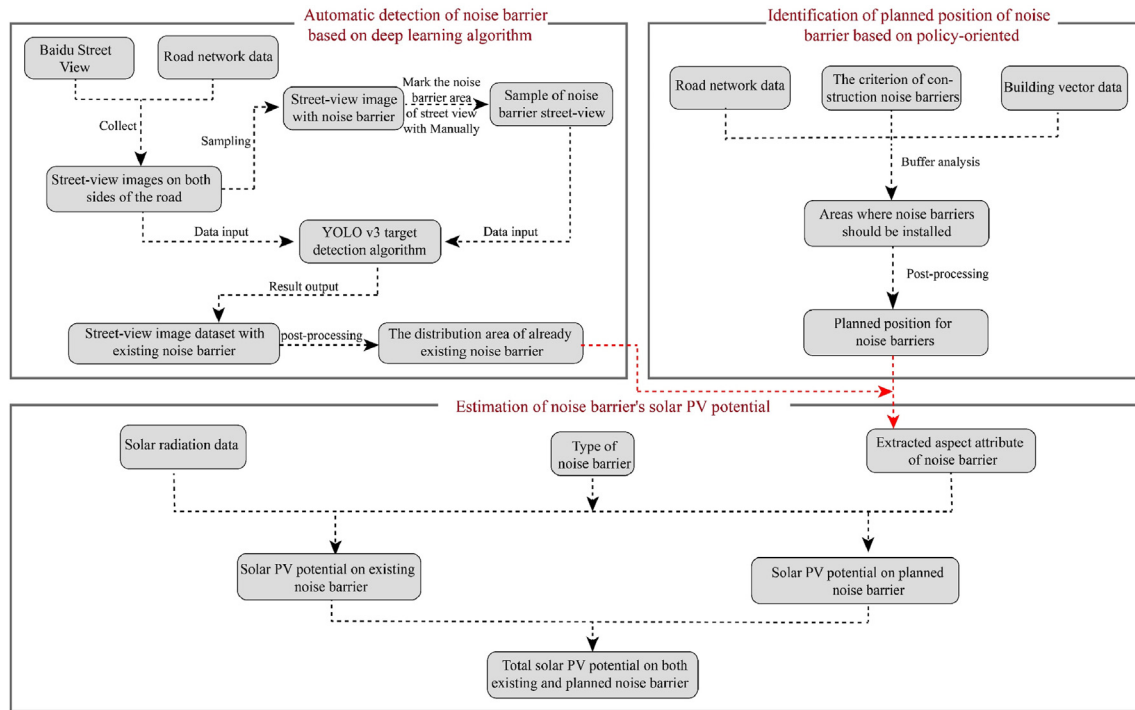


Fig. 1. Research flow chart.

barriers automatically. The street-view images containing noise barriers can be identified from the massive available dataset of street-view images using a YOLO v3 model trained on our custom dataset. The sites of existing noise barriers can then be determined based on the locations where the street-view images containing noise barriers were captured.

YOLO v3 is the third version of this object detection algorithm series. Compared with the previous versions, the accuracy of YOLO v3 is significantly improved, especially for small targets [45]. To train a YOLO v3 model that can be used for noise barrier detection, we labelled noise barriers in street-view images in the experimental area. Model training is based on the training data set composed of street-view images with the noise barriers marked. Finally, a weight file is generated containing noise barrier feature information. This weight file can be used to identify images containing noise barriers from among all the street-view images. The working principle of this approach is shown in Fig. 4. The input street-view images were first divided into several grids of uniform size. Each grid was used to predict the targets within it. Then, for each grid, several prediction boxes were proposed that may contain noise barriers along with their corresponding confidence levels. The basis for determining whether there is a noise barrier in the street-view image is whether the confidence score of the prediction frame exceeds a certain threshold. In this study, this threshold was set to 0.5 based on experience gained from similar studies [46]. This threshold has a good effect for detecting noise barriers in street-view images. Finally, the sampling points with noise barriers were mapped to the corresponding roads and serialized to complete the automatic detection of the existing noise barriers in the study area.

3.4. Identify the planned sites of the noise barrier

The solar PV potential of the planned noise barriers are simulated with regard to the installation of PVNB systems on planned

noise barrier sites. In this section, planned noise barrier sites are identified based on the urban provisions for noise barrier installation and urban environmental noise standards [47,48]. According to the urban policy, noise barriers should be planned for installation when a road passes within a 35-m radius of buildings. As shown in Fig. 5, a point (Point A) is set at the edge of the building. Then, a vertical line is drawn to the road closest to the building; the vertical line crosses the road at Point B. A noise barrier site should be planned when the distance (L) between Point A and Point B is less than 35 m.

After identifying the planned sites for noise barriers based on the buffer analysis, the identification results are further processed by removing sites where noise barriers already exist from the results. The overall framework and working process are shown in Fig. 6.

ArcGIS was used first during the task of identifying planned positions noise barrier sites to create a 35-m buffer zone around the buildings in the study area (the yellow area in Fig. 5). The next step was to find the overlaps between the 35-m building buffer and the road network to find roads where noise barriers need to be established (the orange area in Fig. 5). Finally, the identification results were post-processed to identify errors and modify and optimize discontinuous results in the initial results. Finally, positions with existing noise barriers acquired in 3.2 were removed. The final outcome of the planned site identification for noise barriers is exemplified by the white dotted line in Fig. 5.

3.5. Estimation of solar PV potential based on the identified PVNB system sites

The solar PV potential based on the identified site for the PVNB system were estimated using a computational solar radiation model. Different types of noise barriers have different structures. In this study, to simplify the estimation process, only the factors that have a large influence on solar radiation are considered: these

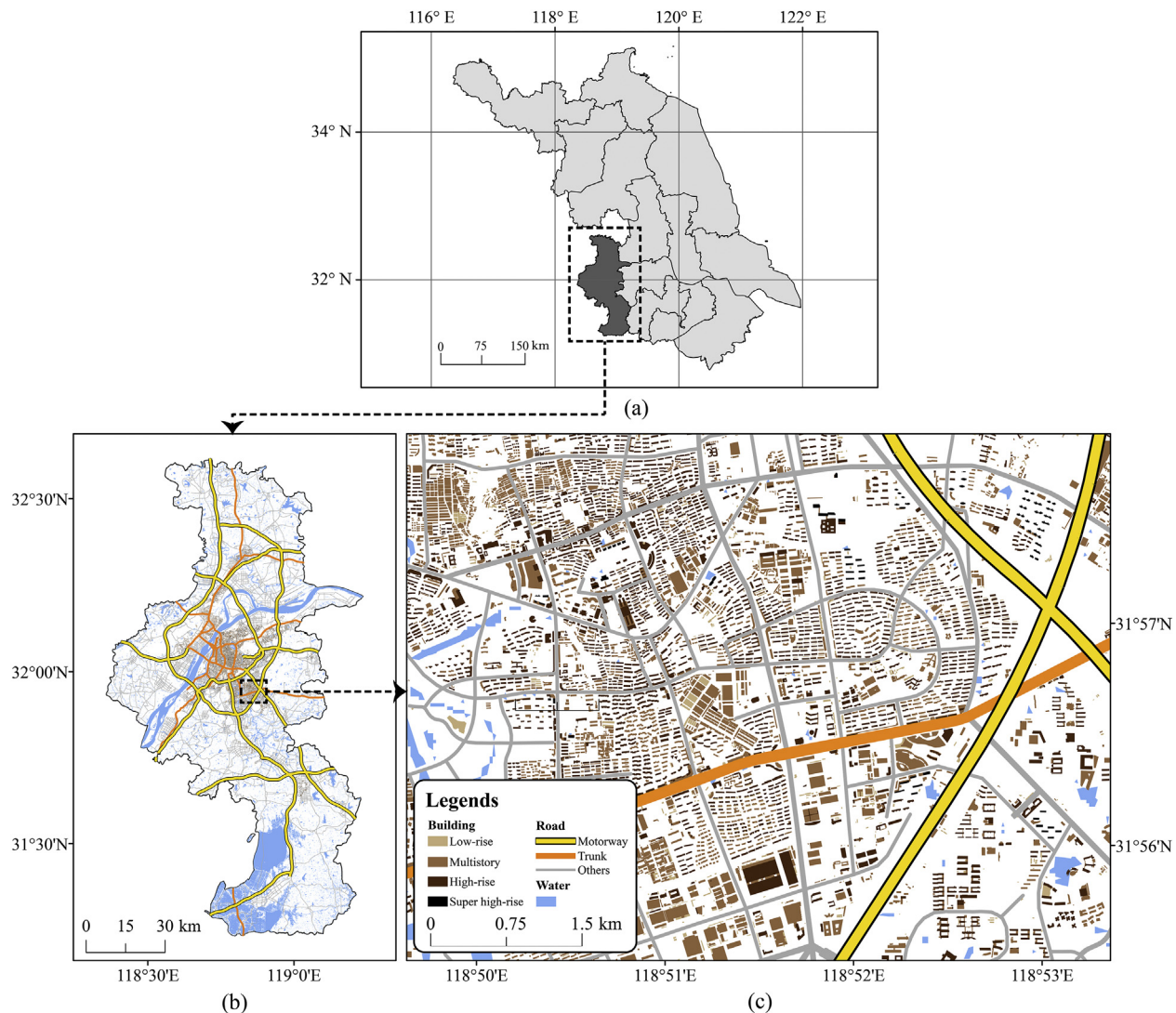


Fig. 2. Study area and experimental data. (a) and (b) show the location of the study area, (c) is the magnified area in the main urban area of Nanjing in (b) to give an illustration of the experiment data.



Fig. 3. An illustration of the street-view imagery captured in four directions at two sample sites.

include slope, orientation, area, and latitude. The estimation of solar PV potential for the identified sites for the PVNB system is based on the following assumptions. This study assumes that the

existing types of noise barriers in Nanjing are vertical and that all the noise barriers are 3 m tall. Considering that reflections from PV modules installed on the PVNB can cause driver distraction on

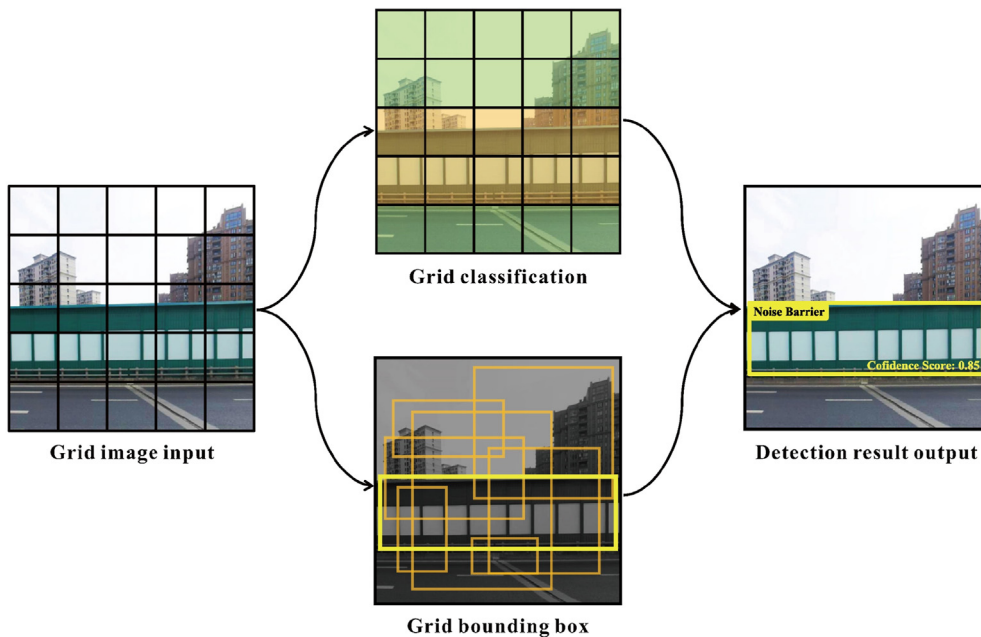


Fig. 4. Schematic diagram of the process of automatic detection of noise barriers based on street-view images.

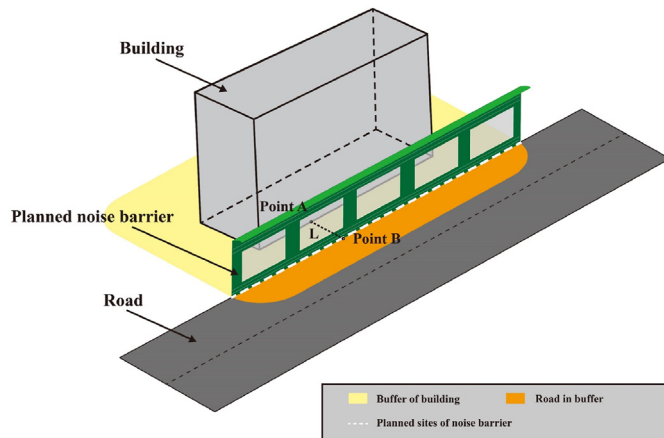


Fig. 5. Schematic diagram of the planned sites of the noise barrier.

roadways, this study assumes that the PV modules to be installed on the noise barrier are installed on the side of the barrier away from the road surface. Based on this assumption, the inclination angle parameter (90°) and height parameter (3 m) of the noise barrier are determined. Then, the noise barrier orientation and latitude information are obtained based on the results of the automatic detection of both the existing and planned noise barriers.

Several steps are involved in assessing the solar PV potential of a location: First, geographical and meteorological data, such as building outlines, LiDAR, aerial satellite imagery, radiometric data from land or satellite sites, etc. is entered. Second, a radiation model combined with GIS analysis is used to obtain a radiation estimate. Third, interfaces by which users can query, operate, and evaluate the solar radiation potential at different levels are developed [49]. Many models have been developed to estimate solar radiation; these vary in complexity—from simple empirical formulas based on ordinary weather or climate data to complex solar radiation transfer models [50]. Angstrom-Prescott formula describes the ratio of total atmospheric transmittance to hours of sunshine and the

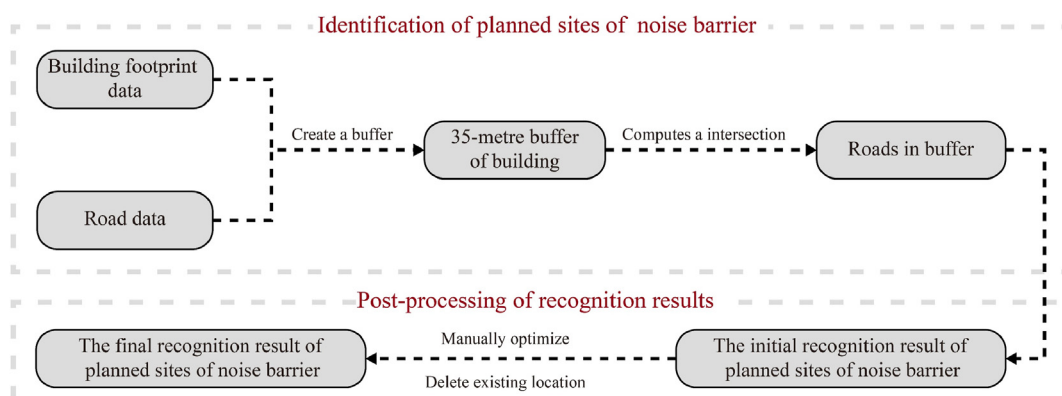


Fig. 6. Flowchart of the identification of the planned sites of the noise barrier.

total outside sunshine hours as a linear relationship [51]. The Hardgreaves–Samani model has been widely applied in calculating the total atmospheric transmittance with daily temperature changes [52]. For real terrain at large spatial and time scales, solar radiation estimation can be performed only through numerical models that simulate the physical environment. Different software tools consider various influencing factors and apply different technical methods. For example, ArcGIS Solar Analyst considers factors such as location, altitude, direction, and atmospheric transport [28], while the r.sun model uses data such as terrain, latitude, turbidity, radiation, and precise sky index to estimate the amount of radiation on a horizontal or inclined surface [53].

For this study, based on the known surface-level radiation data, a horizontal and inclined plane solar radiation conversion model was used to estimate whether solar radiation available at a noise barrier in the study area was sufficient.

The calculation process of solar PV potential for the noise barriers is shown in Fig. 7. Based on the clear sky surface radiation data from CAMS (<http://www.soda-pro.com/web-services/radiation/cams-radiation-service>), the pre-processing extracts Global Horizontal Irradiation (GHI), Beam Horizontal Irradiation (BHI), and Diffuse Horizontal Irradiation (DHI) components to generate radiation data that can be used for the estimation. For the pre-determined research period, the solar position information was calculated and updated at 15-min intervals. Then, the data were entered into the solar radiation estimation model to obtain the total amount of solar radiation received in a single interval. Finally, after calculating the solar PV potential for the entire study period, the results were accumulated to obtain the total solar PV potential of the noise barriers. The locative relationship between incident sunlight and a noise barrier is illustrated in Fig. 8.

The solar radiation reaching an inclined ground surface consists of two parts: direct beam radiation and diffuse radiation, as shown in Fig. 9. The reflected radiation is not considered in this study because it constitutes only a small proportion of the total radiation. Equation (1) is applied to calculate the global radiation [54]:

$$GI_{\beta\gamma} = DBI_{\beta\gamma} + DI_{\beta\gamma} \quad (1)$$

where β is the slope angle of the noise barrier, γ is the azimuth angle of the noise barrier, $GI_{\beta\gamma}$ is the global radiation, $DBI_{\beta\gamma}$ is the direct beam radiation, and $DI_{\beta\gamma}$ is the diffuse radiation, as introduced in Section 3.5.

Equation (2) is applied to calculate $DBI_{\beta\gamma}$ in Equation (1) [55]:

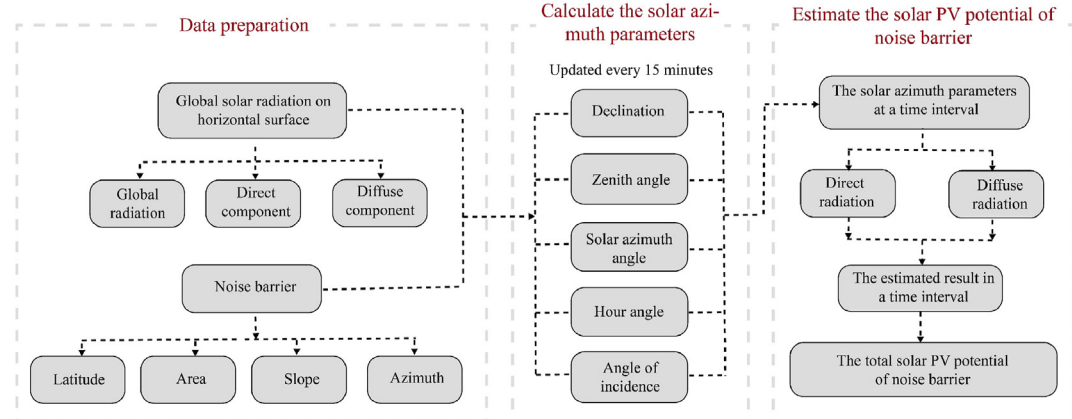


Fig. 7. Flowchart of the estimation of solar PV potential for the noise barriers.

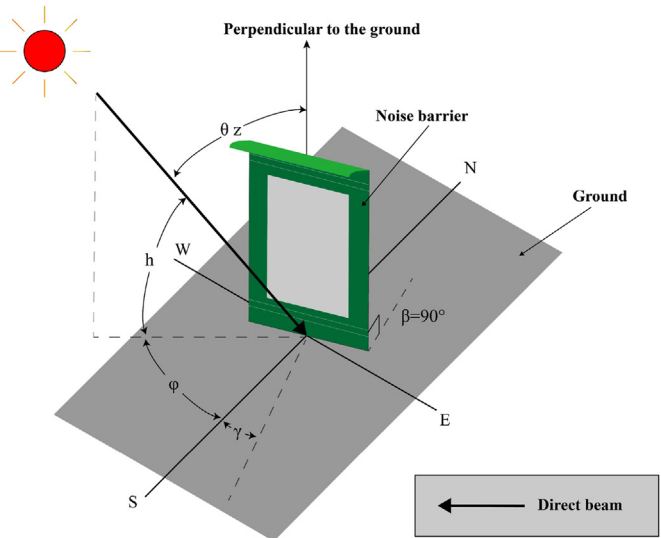


Fig. 8. Schematic diagram of the locative relationship between incident sunlight and a noise barrier, where β is the slope angle of the noise barrier, γ is the azimuth angle of the noise barrier, ϕ is the azimuth angle of the sun, θ_z is the zenith angle of the sun, and h is the altitude angle of the sun.

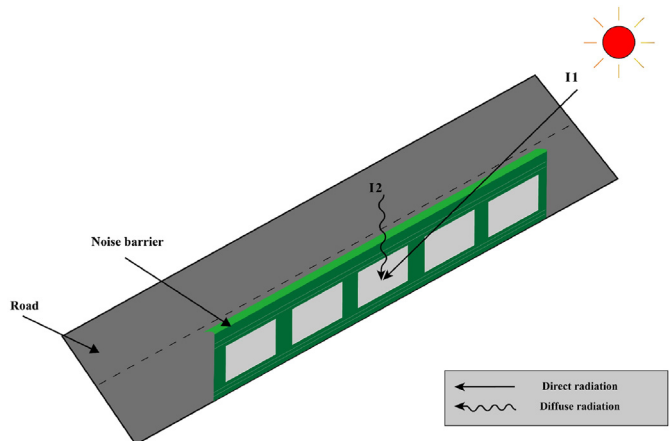
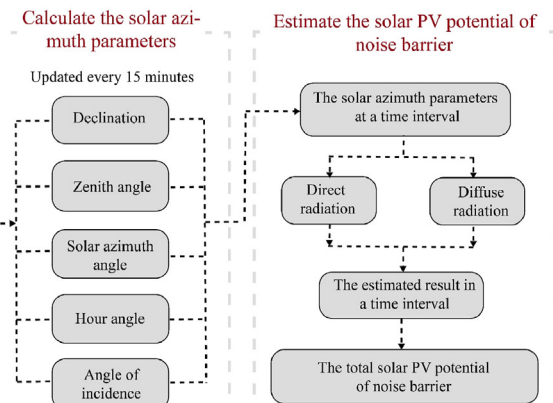


Fig. 9. Schematic diagram of the solar radiation received by a noise barrier. I1 denotes direct radiation, and I2 denotes diffuse radiation.



$$DBI_{\beta\gamma} = BHI \times R_b \quad (2)$$

where BHI is the beam radiation on the horizontal surface and R_b is the beam radiation conversion factor, that is, the ratio of the beam radiation on an inclined surface to that on a horizontal surface of the solar panel.

$$R_b = \max\{[\cos \beta \times \sin h + \sin \beta \times \cos h \times \cos(\phi - \gamma)] / \cos \theta_z, 0\} \quad (3)$$

where β is the slope angle of the noise barrier, h is the altitude angle of the sun, ϕ is the azimuth of the sun, γ is the azimuth angle of the noise barrier, and θ_z is the solar zenith angle ($\theta_z = 90^\circ - h$).

$DI_{\beta\gamma}$ cannot be obtained directly; instead, it needs to be calculated based on the horizontal diffuse radiation, as follows [56]:

$$DI_{\beta\gamma} = DHI \times \left\{ (1 - K_b) \times (1 + \cos \beta) / 2 \times \left[1 + f \times \sin^3 \left(\frac{\beta}{2} \right) + K_b \times R_b \right] \right\} \quad (4)$$

where K_b and f are the anisotropy indexes of the diffuse radiation and DHI is the diffuse radiation on a horizontal surface.

The calculation formulas are as follows:

$$K_b = \min \left[\frac{(GHI - DHI)}{I_0}, 1 \right] \quad (5)$$

$$f = (DNI/GHI)^{0.5} \quad (6)$$

where GHI is the global radiation on the horizontal surface, DNI is the direct normal radiation, and I_0 is the extraterrestrial irradiance in an horizontal surface.

The radiation data obtained in this research are for clear sky conditions; consequently, the effect of cloud cover on solar radiation under real weather conditions still needs to be considered. This study refers to the relevant model proposed by Huang to calculate the monthly average atmospheric transmittance and diffuse ratio using cloud cover data [57]. Meteorological data for sunny and cloudy days in the study area were obtained from World Weather Online (<https://www.worldweatheronline.com/>). Then, the total solar radiation received by the noise barrier under actual weather conditions was calculated.

$$M_{trans} = 0.7 \times P_{clear} + 0.3 \times P_{cloudy} \quad (7)$$

$$M_{dif} = 0.2 \times P_{clear} + 0.7 \times P_{cloudy} \quad (8)$$

where M_{trans} is the monthly average atmospheric transmittance, M_{dif} is a monthly average diffuse ratio, P_{clear} is the percentage of clear days in each month, and P_{cloudy} is the percentage of monthly cloudy weather.

Therefore, the total solar radiation received by the noise barrier under actual weather conditions is $GI_{\beta\gamma}^i$:

$$GI_{\beta\gamma}^i = \sum_{m=1}^{12} \left(\sum_{d=1}^{n_2} \left(\sum_{h=5}^{20} DBI_{\beta\gamma} \right) \times M_{trans} \right) + \sum_{m=1}^{12} \left(\sum_{d=1}^{n_2} \left(\sum_{h=5}^{20} DBI_{\beta\gamma} \right) \times M_{dif} \right) \quad (9)$$

where $GI_{\beta\gamma}^i$ is i -th noise barrier received total solar radiation in a year, and i is the i -th noise barriers ($i = 1, 2, 3, \dots, n_1$), m represents month ($m = 1, 2, 3, \dots, 12$), Here, d is d -th day of the month, n_2 is the actual number of days in each month, h is the time in a 24-h system ($h = 5, 6, 7, \dots, 20$).

The following formula is applied to estimate the total solar radiation potential (TSR) of all the noise barriers in Nanjing for each full year:

$$TSR = \sum_{i=1}^{n_1} (S_i \times GI_{\beta\gamma}^i) \quad (10)$$

where S_i is the area of the i -th noise barrier, i is the number of noise barriers ($i = 1, 2, 3, \dots, n_1$), where n_1 is the total number of noise barriers, and TSR is the total solar PV potential of the PVNB system for one year (MWh).

3.6. Estimation of solar PV power generation based on the identified PVNB system sites

The estimation of solar PV potential is crucial for accurate measurement of the installed capacity of the PVNB system. To harvest the largest amount of the electricity of the PVNB system, the rated power of the installed solar panel is selected according to the maximum solar radiation power of the noise barrier in this area. The noise barrier in the area with the largest annual solar radiation reception is used to calculate the maximum solar radiation received by the noise barrier in this area per unit area and unit time. In this study, the specifications of the installed solar panels were determined to have a dimension of 1 m × 1 m with a rated power of 200 W. The total power generation of the PVNB system in Nanjing can be calculated using Equation (11) [58]:

$$E_P = P_{AZ} \times H \times K \quad (11)$$

where E_P is the power generation of solar PV electricity (kWh), P_{AZ} is the installed capacity of the solar PV system (kW), H is the average peak sunlight hours of the solar PV system (h), K is the overall performance coefficient of the solar PV system with general value of 0.8 [59].

The average peak sunlight hours can be calculated by Equation (12) [58].

$$H = \frac{TSR}{S \times E_s} \quad (12)$$

where TSR is the total solar radiation potential of all the noise barriers, and S is the area of solar panels laid on the noise barriers, E_s is the standard test condition of photovoltaics (= 1000 W/m²).

The installed capacity of the solar PV system is calculated with the rated power P of a single solar panel and the number N of solar panels of the solar PV system using Equation (13) [60]:

$$P_{AZ} = P \times N \quad (13)$$

where P is the rated power of one single solar panel, and N is the number of solar panels.

4. Experimental results

This study adopted Nanjing as a study area to verify the automatic method for detecting noise barriers and identifying the potential radiation. The overall assessment of the noise barriers' solar PV potential was implemented to construct an economic evaluation of the utility of noise barriers to investigate their potential for application.

4.1. Solar PV potential of existing noise barriers

Based on the methodology of automatic detection of noise

barriers described in Section 3.2, a total of 72,399 street-view images of the road networks (motorway and trunk roads) in Nanjing were obtained. Based on the previous sampling results of noise barriers, 1289 street-view images containing noise barriers and 100 street-view images containing tunnels were selected from the current sampling points of noise barriers in Nanjing through visual inspection. The noise barriers and the inner walls of the tunnels were labelled separately because, during a preliminary test, street-view images with tunnels and some other areas were easily mistaken as noise barriers. Therefore, the street-view images with the tunnels treated as a separate detection target. The street-view image samples with labelled noise barriers and tunnels were input into the YOLO v3 model for training. After obtaining the weight file, all the street-view images were input into the model for detection, finally achieving the automatic detection of noise barriers in Nanjing. The output street-view images of the model were divided into three categories: 2250 street-view images contained noise barriers, 1812 contained tunnels, and 68,337 contained no noise barriers and tunnels.

The accuracy indicators were used to evaluate the recognition accuracy of the model. From the complete set of 72,339 street-view images of the automatic noise barrier detection model, 20% (14,481 images) were selected from each of the three types of output datasets and used to test model accuracy. Among the 450 street-view images contained noise barriers, there are 316 images detected correctly and 134 images detected incorrectly. Among the 363 street-view images with tunnels, 362 images are detected correctly, and 1 image is detected incorrectly. Among the 13,668 street-view images that contain neither the noise barrier nor the tunnel, 13,256 images are detected correctly, and 412 images are detected incorrectly. For the total 14,481 sampling images, there are 13,934 images detected correctly and 547 images are detected incorrectly. Therefore, the accuracy of the automatic noise barrier detection model in our case study is 96.22%.

The coordinates of the street-view images that were finally detected as containing noise barriers were mapped to the road layer and serialized processing. In this study, we determine the distribution of existing noise barriers according to the identification results based on the street-view images. Street-view images were obtained at sample points of 20 m intervals. The road section will be determined to have noise barrier installed if two continuous street-view images are both identified to have contained noise barriers. The spatial distribution of the existing noise barriers in Nanjing was obtained, as shown in Fig. 10:

As Fig. 10 shows, the existing noise barriers in Nanjing appear mainly in scattered areas with dense buildings around the trunk roads near the centre of the city, such as areas A and B in Fig. 10. These areas are relatively close to trunk roads, and residents will be significantly affected by road noise pollution. It is necessary to establish noise barriers in these areas to reduce traffic noise to ensure a better living environment. Another feature is that the noise barrier fragments distributed on both sides of truck routes are more critical. At present, there are few noise barriers on both sides of any motorway in Nanjing, except for those distributed in small concentrated areas, for example, the C area. The motorway network in Nanjing is mainly distributed around the peripheral areas of the city. The traffic noise from these motorways does not seriously affect urban residents because of the long distances between the motorways and the nearest residential areas; therefore, noise barriers are less common on highways. However, due to the relatively dense distribution of buildings on both sides of the Nanjing motorway, the total length of the noise barriers distributed along both sides of the motorway in this area is longer.

The urban building surface model was constructed in ArcGIS based on the height attributes of the building vector data. Then, the

ArcGIS Mountain Shadow Tool was used to calculate the shadows caused by urban buildings. The shadow layer was overlaid with the noise barrier location layer to determine the effect of urban building shadows on the estimation of the solar PV potential on the noise barriers. This analysis found that the noise barriers in Nanjing are not covered by shadows from the surrounding buildings.

Based on the statistics of the extent of existing noise barriers along motorway and trunk roads in Nanjing, the total mileage of the existing noise barriers in Nanjing is 23,767 m. Among these, the extents of the noise barriers on motorway and trunk roads are 14,558 m and 9209 m, respectively.

Using the solar radiation data and the method for estimating the solar radiation potential of inclined surfaces described in Section 3.5, the PV potential of existing noise barriers in Nanjing was estimated. According to the acquired GHI and DNI data of Nanjing with a 15-min update rate in 2019 as introduced in Section 3.5, we calculated the annual solar radiation received by each existing noise barrier during this time period. Then the solar PV potential of the existing noise barriers of Nanjing in 2019 was derived by summing the cumulative power generation for all of 2019. The visualized results are shown in Fig. 11:

As Fig. 11 shows, the areas with large noise barrier solar PV potential are largely consistent with the concentrated distribution area of noise barriers from Fig. 10. However, the solar PV potential of the noise barriers in areas A and C is significantly higher than that in area B. This is because the distribution of noise barriers in areas A and C has strong continuity; moreover, the area where solar PV modules can be installed is relatively larger. Although area B is where the distribution of noise barriers is concentrated, noise barriers are not continuously distributed. Therefore, the solar PV potential of noise barriers in area B is lower than that in areas A and C. According to Fig. 10, the existing noise barriers in Nanjing are mainly distributed on the trunk roads in the city, and there are few distributed on both sides of the motorway. However, Fig. 11 shows that the solar PV potential of the existing noise barriers on the motorway in Nanjing is concentrated in some areas. The results indicated that the annual PV potential on the existing site of the noise barrier of motorway and trunk roads in Nanjing are 18,015 MW h and 11,122 MW h, respectively.

4.2. Solar PV potential of planned noise barrier

Fig. 12 shows the spatial distribution of noise barriers in Nanjing based on policy simulation is emphatically correlated with the distribution of urban buildings. Almost all the sections of buildings surrounding both sides of the trunk roads were identified as locations where noise barriers should be built, such as areas A and B in Fig. 12. According to the specifications for noise barriers installation, it is necessary to establish noise barriers within a certain range of different building categories in urban areas, such as residential areas, hospitals, and commercial areas. The purpose is to improve the quality of the acoustic environment and ensure appropriate volume levels for residential living, study, and work areas. The trunk roads in the city are generally close to this area; consequently, many areas exist where noise barriers need to be installed. Unlike the trunk roads in the city, there are fewer areas where noise barriers need to be installed on the Nanjing motorway. Except for the relatively concentrated distribution in area C, other areas have sparser distributions. Through the statistics on the noise barrier mileage based on policy simulation in Nanjing, we found that the total extent of planned noise barriers in Nanjing is 95,390 m. Among these, noise barrier extents of motorways and trunk roads are 12,925 m and 82,465 m, respectively.

The process of solar PV potential assessment based on policy simulation was performed consistently with the process of solar PV

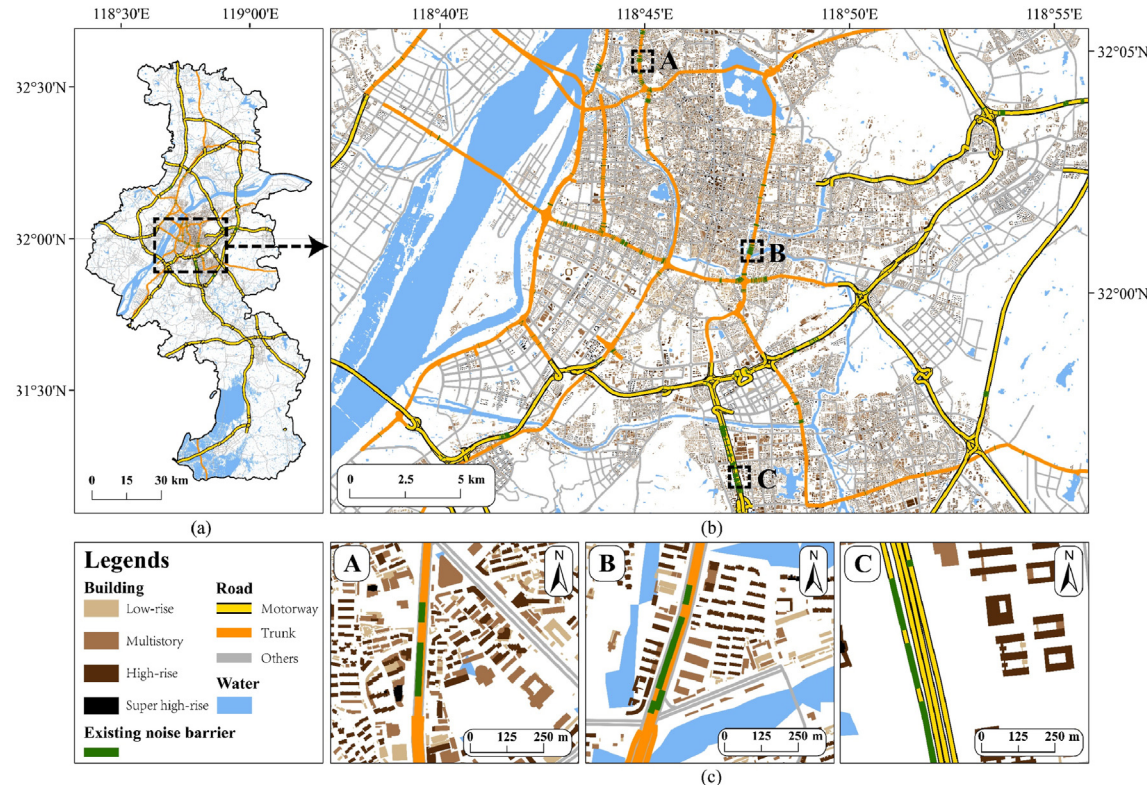


Fig. 10. The automatic detection result of existing noise barriers in Nanjing. (a) An overview of the spatial distribution of existing noise barriers in Nanjing with dash line box marked the part of the magnified area; (b) The magnified area in the main urban area of Nanjing; (c) The partial detail display of the marked three areas in Fig. 10 (b).

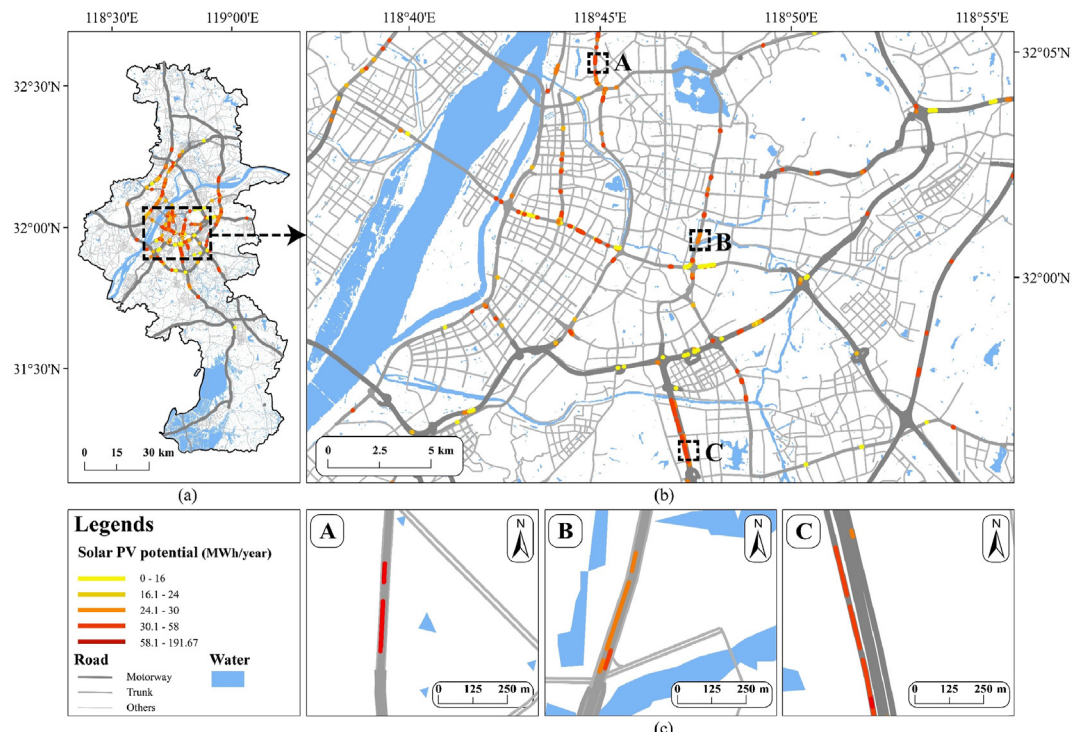


Fig. 11. Spatial distribution of solar PV potential of the existing noise barriers in Nanjing. (a) An overview of the solar PV potential of the existing noise barriers in Nanjing with dash line box marked the part of the magnified area; (b) The magnified area in the main urban area of Nanjing; (c) The partial detail display of the marked three areas in Fig. 11 (b).

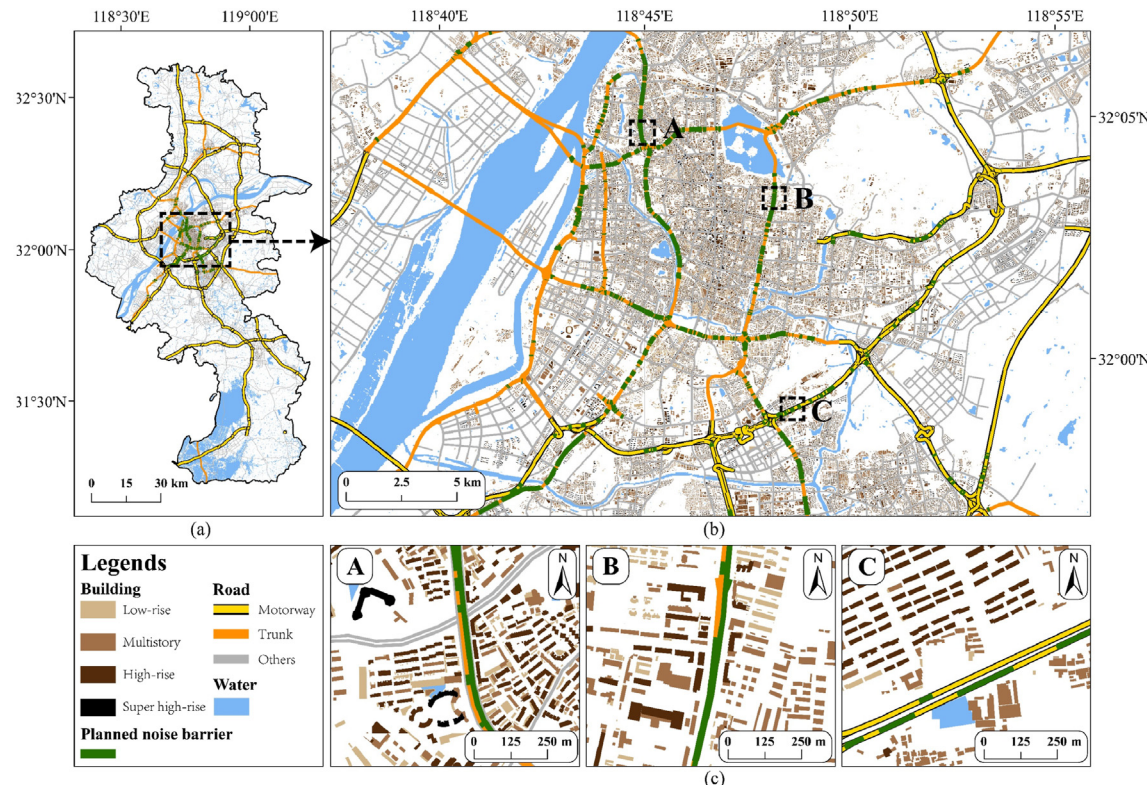


Fig. 12. Spatial distribution of planned noise barriers in Nanjing. (a) An overview of the spatial distribution of planned noise barriers with dash line box marked the part of the magnified area; (b) The magnified area in the main urban area of Nanjing; (c) The partial detail display of the marked three areas in Fig. 12 (b).

potential assessment for the existing noise barriers in Nanjing. The solar radiation received by each noise barrier during the study period was calculated according to the acquired GHI and DNI data of Nanjing City updated every 15 min in 2019, as introduced in Section 3.5. Then the solar PV potential of the planned noise barrier in Nanjing in 2019 was calculated by summing the cumulative radiation for the entire year. The calculation results are visualized in Fig. 13:

Fig. 13 shows that the area with the highest solar PV potential is consistent with the concentrated distribution area of noise barriers in Fig. 12. In particular, noise barriers along Nanjing's trunk roads have substantial solar PV potential, especially in areas A and B. In addition, the noise barriers are widely distributed on both sides of the trunk roads in other areas. The distribution of solar PV potential based on policy simulation along the Nanjing motorway is also relatively extensive. In addition to the relatively concentrated delivery in the C area, other areas possess specific distributions. According to the solar PV potential statistics, the annual solar PV potentials of noise barriers based on planned sites along Nanjing's motorway and trunk roads are 15,241 MW h and 97,811 MW h, respectively.

4.3. Temporal analysis of solar PV potential

This study also performed a time series analysis of the solar PV potential for all the solar barriers in both the existing and planned locations. The total solar PV potential the existing and planned noise barriers in Nanjing during different periods of each month of the year was estimated, and the results are shown in Table 1. Specifically, according to the seasonal characteristics of the hourly solar PV potential of each noise barrier, we divided the hourly solar PV potential curve into different colours by month as follows: (i) spring

(green): March, April, and May; (ii) summer (red): June, July, and August; (iii) autumn (orange): September, October, and November; (iv) winter (blue): December, January, and February.

Fig. 14 illustrates the overall solar PV potential of the all noise barrier of Nanjing changes at different times in one day. The solar PV potential peaked at 11 a.m., and 3 p.m. as the noise barriers are placed vertically on both sides of the road. This condition differs from the characteristics of solar radiation received on a horizontal plane. When the receiving surface of the solar panel is horizontal, the acceptable direct radiation intensity is highest when the solar elevation angle reaches its maximum value at noon. On the contrary, when the receiving surface of the solar panel is vertical with a fixed orientation, the optimal light incidence angle will not occur at noon. For example, in winter at 7–8 am o'clock, the solar radiation received by PVNB are higher than other time in the noon as the solar radiation just hits the PVNB vertically.

Because of the different sunrise and sunset times on each day of the year, the received radiation in certain months is zero from 5 to 7 am, and from 5 to 8 pm. By comparing the sum calculated for each month, it can be seen that the solar PV potential of the noise barrier reaches a maximum of 13,562 MW h in July and a minimum of 9617 MW h in January. Generally, the PV potential is substantial between April and September but weak in winter (i.e., November December, January, and February).

4.4. Solar PV power generation of existing and planned PVNB

The potential installed capacity of the PVNB system and the average peak sunlight hours in Nanjing can be calculated according to the solar power generation estimation method described in Section 3.6. The measured potential installed capacity and average peak sunlight hours can further be used to estimate the power

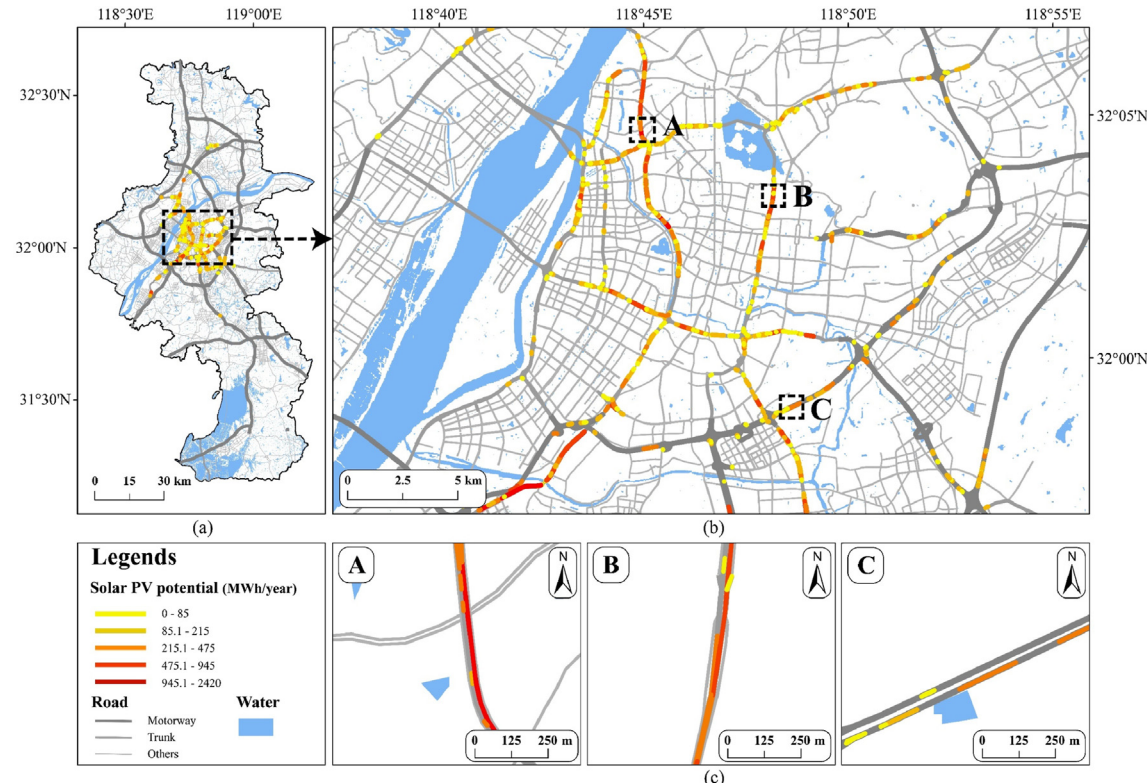


Fig. 13. Spatial distribution of the solar PV potential of planned noise barriers in Nanjing. (a) An overview of the solar PV potential of planned noise barriers in Nanjing with dash line box marked the part of the magnified area; (b) The magnified area in the main urban area of Nanjing; (c) The partial detail display of the marked three areas in Fig. 13 (b).

Table 1

Solar PV potential of existing and planned PVNB system in Nanjing during different periods of each month in 2019 (MWh).

Month	5~6am	6~7am	7~8am	8~9am	9~10am	10~11am	11am~12pm	12~1pm	1~2pm	2~3pm	3~4pm	4~5pm	5~6pm	6~7pm	7~8pm	Total
January	0	0	393	674	967	1107	1149	1167	1184	1140	957	824	54	0	0	9617
February	0	8	287	712	972	1081	1112	1161	1248	1295	1220	1019	256	0	0	10,371
March	0	308	638	969	1123	1139	1080	1060	1167	1272	1239	978	571	8	0	11,553
April	41	352	758	993	1071	1042	966	1024	1215	1383	1443	1305	998	166	0	12,756
May	502	728	1015	1110	1080	959	790	732	981	1225	1355	1271	879	270	0	12,895
June	618	738	994	1075	1034	912	742	617	852	1104	1245	1188	858	302	1	12,279
July	301	655	976	1115	1143	1100	1006	948	1127	1300	1373	1270	913	336	0	13,562
August	71	480	888	1077	1121	1079	997	1027	1208	1363	1424	1311	930	392	0	13,367
September	3	894	937	1121	1156	1098	1008	1019	1161	1288	1285	1057	694	0	0	12,721
October	0	449	739	1076	1183	1156	1080	1078	1165	1190	1018	568	333	0	0	11,035
November	0	43	1261	1091	1194	1182	1131	1124	1153	1108	870	492	0	0	0	10,649
December	0	0	1016	956	1152	1195	1159	1115	1092	997	711	226	0	0	0	9618
Total	1535	4655	9902	11,970	13,196	13,048	12,221	12,070	13,553	14,664	14,140	11,508	6487	1473	1	140,423

generation of both the existing and planned urban noise barriers in Nanjing.

The total available area on the existing noise barriers for installing the solar panel is 71,303 m², while the total available area on the planned noise barriers for installing the solar panel is 286,175 m². In this study, the installed solar panels are in a dimension of 1 m × 1 m with a rated power of 200 W. For the existing urban noise barriers, the potential installed capacity of the PVBN system in year 2019 is 14.26 MW, and the average peak sunlight hours is 408.65 h. Therefore, the potential total power generation of the PVBN system based on the existing urban noise barriers is 4662 MW h in 2019. For the planned urban noise barriers, the potential installed capacity of the PVBN system in year 2019 is 57.24 MW, and the average peak sunlight hours is 395.05 h. Therefore, the potential total power generation of the PVBN

system based on the planned urban noise barriers is 18,088 MW h in 2019.

5. Conclusion and future studies

This study provided a computational method for estimating solar PV potential based on noise barriers. Nanjing was used as a case study to demonstrate the efficiency of the estimation process. Using a deep learning-based target detection method, we first identified sites with existing urban noise barriers from massive numbers of street-view images. The accuracy of noise barrier detection by this system reached 96.22%. Both the existing and planned sites of the urban noise barrier are selected as potential sites for installing the PVNB system. Based on the existing and planned locations of noise barriers in Nanjing, the annual solar PV

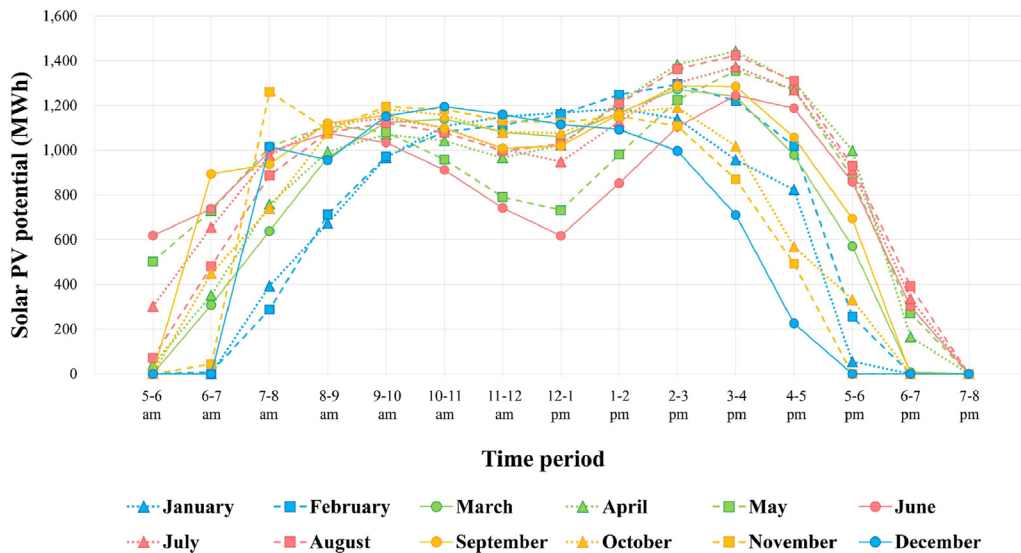


Fig. 14. Solar PV potential of existing and planned PVNB systems in Nanjing during each month in 2019.

potentials in year 2019 are 29,137 MW h and 113,052 MW h, and the potential solar PV power generations in 2019 are 4662 MW h and 18,088 MW h, respectively. The estimation results of solar PV potential of PVNB systems are calculated based on the automatic noise barrier detection model in Nanjing and the solar radiation data of Nanjing in 2019 provided by Copernicus Atmosphere Monitoring Service (CAMS), which can be further improved with more accurate noise barrier detection model and meteorological data.

The method developed in this study is highly flexible and can be applied to other regions of the world. To simplify the estimations, this study assumed that PVNB has only one size. The cost involved in manufacturing the PV modules has declined rapidly in recent years, which enables PVNBs to be manufactured with various sizes to meet various local requirements. Future studies could further explore the solar PV potential of noise barriers while considering different sizes and designs. In addition, this study did not consider the economic costs involved in the deployment of PVNB systems. Future work needs to assess the economic feasibility by comparing the cost required to deploy PVNB systems with the potential economic benefits solar PV.

CRediT authorship contribution statement

Teng Zhong: Methodology, Investigation, Writing - original draft, Project administration. **Kai Zhang:** Formal analysis, Investigation, Writing - original draft. **Min Chen:** Conceptualization, Methodology, Supervision, Writing - review & editing, Funding acquisition. **Yijie Wang:** Software, Formal analysis, Visualization. **Rui Zhu:** Writing - review & editing. **Zhixin Zhang:** Investigation, Visualization. **Zixuan Zhou:** Investigation, Visualization. **Zhen Qian:** Software, Visualization. **Guonian Lv:** Writing - review & editing, Supervision. **Jinyue Yan:** Writing - review & editing, Supervision.

Declaration of competing interest

The authors declare that they have no known competing financial interests or personal relationships that could have appeared to influence the work reported in this paper.

Acknowledgments

This work was supported by the National Key Research and Development Program of China (Grant 2017YFB0503500), National Research Foundation Singapore.

References

- [1] W. Hermann, Quantifying global exergy resources, *Energy* 31 (2006) 1685–1702.
- [2] K. Sahu, Bikash, A study on global solar PV energy developments and policies with special focus on the top ten solar PV power producing countries, *Renew. Sustain. Energy Rev.* 43 (2015) 621–634.
- [3] B. Mashhoodi, D. Stead, A. Timmeren, Spatial homogeneity and heterogeneity of energy poverty: a neglected dimension, *Spatial Sci.* 25 (2019) 19–31.
- [4] A. Chow, S. Li, A.S. Fung, Modeling urban solar energy with high spatiotemporal resolution: a case study in Toronto, Canada, *Int. J. Green Energy* 13 (2016) 1090–1101.
- [5] D. Brett, Doltera, Martin Boucherb, Solar energy justice: a case-study analysis of Saskatchewan, Canada, *Appl. Energy* 225 (2018) 221–232.
- [6] E. De Schepper, S. Van Passel, J. Manca, T. Thewys, Combining photovoltaics and sound barriers – a feasibility study, *Renew. Energy* 46 (2012) 297–303.
- [7] K. Bódis, I. Kougias, A. Jäger-Waldau, N. Taylor, S. Szabó, A high-resolution geospatial assessment of the rooftop solar photovoltaic potential in the European Union, *Renew. Sustain. Energy Rev.* 114 (2019).
- [8] Y. Yang, P.E. Campana, B. Stridh, J.Y. Yan, Potential analysis of roof-mounted solar photovoltaics in Sweden, *Appl. Energy* 279 (2020) 115786.
- [9] M. Gu, Y. Liu, J. Yang, L. Peng, C. Zhao, Z. Yang, et al., Estimation of environmental effect of PVNB installed along a metro line in China, *Renew. Energy* 45 (2012) 237–244.
- [10] S.R. Wadhwani, J.M. Pearce, Power and energy potential of mass-scale photovoltaic noise barrier deployment: a case study for the U.S., *Renew. Sustain. Energy Rev.* 80 (2017) 125–132.
- [11] G.N. Lu, B. Michael, S. Josef, H. Lin, A.X. Zhu, M. Chen, Reflections and speculations on the progress in Geographic Information Systems (GIS): a geographic perspective, *Int. J. Geogr. Inf. Sci.* 33 (2019) 346–367.
- [12] H. Lin, M. Chen, Managing and sharing geographic knowledge in virtual geographic environments (VGEs), *Spatial Sci.* 21 (2015) 261–263.
- [13] F.Y. Gong, Z.C. Zeng, E. Ng, L.K. Norford, Spatiotemporal patterns of street-level solar radiation estimated using Google Street View in a high-density urban environment, *Build. Environ.* 148 (2019) 547–566.
- [14] X. Li, C. Ratti, I. Seiferling, Quantifying the shade provision of street trees in urban landscape: a case study in Boston, USA, using Google Street View, *Landsl. Urban Plann.* 169 (2018) 81–91.
- [15] H. Majidifard, Y. Adu-Gyamfi, W.G. Buttler, Deep machine learning approach to develop a new asphalt pavement condition index, *Construct. Build. Mater.* (2020) 247.
- [16] A. Campbell, A. Both, Q. Sun, Detecting and mapping traffic signs from Google Street View images using deep learning and GIS, *Comput. Environ. Urban Syst.* 77 (2019).
- [17] J. Armstrong, A. Ortega, S. Blainey, J. Preston, D. Thompson, G. Squicciarini, et al., Noise reduction for ballasted track: a comparative socio-economic

- assessment, *Int. J. Trans. Dev. Integr.* 3 (2019) 15–29.
- [18] M. Kanellis, M.M. de Jong, L. Slooff, M.G. Debije, The solar noise barrier project: 1. Effect of incident light orientation on the performance of a large-scale luminescent solar concentrator noise barrier, *Renew. Energy* 103 (2017) 647–652.
- [19] U.A. Yusufoglu, T.M. Pletzer, L.J. Koduvvelikulathu, C. Comparotto, R. Kopecek, H. Kurz, Analysis of the annual performance of bifacial modules and optimization methods, *IEEE J. Photovolt.* 5 (2015) 320–328.
- [20] G.J. Faturochman, M.M. de Jong, R. Santergen, W. Folkerts, M. Zeman, A.H.M. Smets, Maximizing annual yield of bifacial photovoltaic noise barriers, *Sol. Energy* 162 (2018) 300–505.
- [21] B. Petter Jelle, C. Breivik, H. Drolsum Røkenes, Building integrated photovoltaic products: a state-of-the-art review and future research opportunities, *Sol. Energy Mater. Sol. Cell.* 100 (2012) 69–96.
- [22] Benjamin Pillota, Nadeem Al-Kurdia, Carmen Gervet, Laurent Lingueta, An integrated GIS and robust optimization framework for solar PV plant planning scenarios at utility scale, *Appl. Energy* 260 (2020) 114257.
- [23] M. Chen, V. Alexey, P.A. Daniel, Albert J. Kettner, et al., Position paper: open web-distributed integrated geographic modelling to enable wider participation and model application, *Earth Sci. Rev.* 207 (2020) 103223.
- [24] G.N. Lu, M. Chen, L.W. Yuan, L.C. Zhou, et al., Geographic scenario: a possible foundation for further development of virtual geographic environments (VGEs), *Int. J. Digital Earth* 11 (2018) 356–368.
- [25] L.K. Wigington, H.T. Nguyen, J.M. Pearce, Quantifying rooftop solar photovoltaic potential for regional renewable energy policy, *Comput. Environ. Urban Syst.* 34 (2010) 345–357.
- [26] L. Niko, Z. Danijel, S. Sebastian, Z. Borut, S. Gorazd, Rating of roofs' surfaces regarding their solar potential and suitability for PV systems, based on LiDAR data, *Appl. Energy* 102 (2013) 803–812.
- [27] A. Verso, A. Martin, J. Amador, J. Dominguez, GIS-based method to evaluate the photovoltaic potential in the urban environments: the particular case of Miraflores de la Sierra, *Sol. Energy* 117 (2015) 236–245.
- [28] P. Fu, P. Rich, Design and implementation of the Solar Analyst: an ArcView extension for modeling solar radiation at landscape scales. Proceedings of the 19th Annual ESRI User Conference, 1999.
- [29] J. Khan, M.H. Arsalan, Estimation of rooftop solar photovoltaic potential using geo-spatial techniques: a perspective from planned neighborhood of Karachi – Pakistan, *Renew. Energy* 90 (2016) 188–203.
- [30] S. Izquierdo, M. Rodrigues, N. Fueyo, A method for estimating the geographical distribution of the available roof surface area for large-scale photovoltaic energy-potential evaluations, *Sol. Energy* 82 (2008) 929–939.
- [31] R. Singh, R. Banerjee, Estimation of rooftop solar photovoltaic potential of a city, *Sol. Energy* 115 (2015) 589–602.
- [32] K. Mainzer, S. Killinger, R. McKenna, W. Fichtner, Assessment of rooftop photovoltaic potentials at the urban level using publicly available geodata and image recognition techniques, *Sol. Energy* 155 (2017) 561–573.
- [33] Z. Huang, T. Mendis, S. Xu, Urban solar utilization potential mapping via deep learning technology: a case study of Wuhan, China, *Appl. Energy* 250 (2019) 283–291.
- [34] L. Bergamasco, P. Asinari, Scalable methodology for the photovoltaic solar energy potential assessment based on available roof surface area: application to Piedmont Region (Italy), *Sol. Energy* 85 (2011) 1041–1055.
- [35] D. Assouline, N. Mohajeri, J.L. Scartezzini, Quantifying rooftop photovoltaic solar energy potential: a machine learning approach, *Sol. Energy* 141 (2017) 278–296.
- [36] J.B. Kodysh, O.A. Omitaomu, B.L. Bhaduri, B.S. Neish, Methodology for estimating solar potential on multiple building rooftops for photovoltaic systems, *Sustain. Cities Soc.* 8 (2013) 31–41.
- [37] D. Anguelov, C. Dulong, D. Filip, C. Frueh, S. Lafon, R. Lyon, et al., Google street view: capturing the world at street level, *Computer* 43 (2010) 32–38.
- [38] S. Freitas, M.C. Brito, Solar façades for future cities, *Renew. Energy Focus* 31 (2019) 73–79.
- [39] TAdL. Martins, L. Adolphe, L.E.G. Bastos, MAdL. Martins, Sensitivity analysis of urban morphology factors regarding solar energy potential of buildings in a Brazilian tropical context, *Sol. Energy* 137 (2016) 11–24.
- [40] X. Li, C. Ratti, Mapping the spatio-temporal distribution of solar radiation within street canyons of Boston using Google Street View panoramas and building height model, *Landscape Urban Plann.* (2019) 191.
- [41] R. Carrasco-Hernandez, A.R.D. Smedley, A.R. Webb, Using urban canyon geometries obtained from Google Street View for atmospheric studies: potential applications in the calculation of street level total shortwave irradiances, *Energy Build.* 86 (2015) 340–348.
- [42] Y. Wang, Y. Tan, W. Zhang, Y. Zhao, X. Kuang, An adversarial attack on DNN-based black-box object detectors, *J. Netw. Comput. Appl.* (2020) 161.
- [43] Q. Chen, P. Wang, A. Cheng, W. Wang, Y. Zhang, J. Cheng, Robust One-Stage Object Detection with Location-Aware Classifiers, *Pattern Recognition*, 2020.
- [44] X. Wu, D. Sahoo, S.C.H. Hoi, Recent advances in deep learning for object detection, *Neurocomputing* 396 (2020) 39–64.
- [45] J. Redmon, A. Farhadi, YOLOv3: An Incremental Improvement, 2018.
- [46] P. Shehan, L.S. Rajendran, R. Pradeep, Sajith Vijayaraghavan, Real-time Traffic Sign Recognition Using YOLOv3 Based Detector, 2019.
- [47] China MoEaEotPsRo, Environmental Quality Standards for Noise, 2008.
- [48] China MoEaEotPsRo, Technical Specifications for Regionalizing Environmental Noise Function, 2014.
- [49] S. Freitas, C. Catita, P. Redweik, M.C. Brito, Modelling solar potential in the urban environment: state-of-the-art review, *Renew. Sustain. Energy Rev.* 41 (2015) 915–931.
- [50] D.G. Goodin, J.M.S. Hutchinson, R.L. Vanderlip, M.C. Knapp, Estimating solar irradiance for crop modeling using daily air temperature data, *Agron. J.* 91 (1999) 845–851.
- [51] A. Angstrom, Solar and terrestrial radiation. Report to the international commission for solar research on actinometric investigations of solar and atmospheric radiation, *Q. J. R. Meteorol. Soc.* 50 (1924).
- [52] M.R. Hasan, Discussion of "estimating potential evapotranspiration" by George H. Hargreaves and Zohrab A. Samani (september, 1982), *J. Irrigat. Drain. Eng.* 109 (1983) 341–343.
- [53] M. Súri, T.A. Huld, E.D. Dunlop, PV-GIS: a web-based solar radiation database for the calculation of PV potential in Europe, *Int. J. Sustain. Energy* 24 (2005) 55–67.
- [54] P.I. Raptis, S. Kazadzis, B. Psiloglou, N. Kouremeti, P. Kosmopoulos, A. Kazantzidis, Measurements and model simulations of solar radiation at tilted planes, towards the maximization of energy capture, *Energy* 130 (2017) 570–580.
- [55] M. Iqbal, An introduction to solar radiation, *Space Sci. Rev.* 39 (1983) 387–390.
- [56] D.T. Reindl, W.A. Beckman, J.A. Duffie, Evaluation of hourly tilted surface radiation models, *Sol. Energy* 45 (1990) 9–17.
- [57] S. Huang, P.M. Rich, R.L. Crabtree, C.S. Potter, P. Fu, Modeling monthly near-surface air temperature from solar radiation and lapse rate: application over complex terrain in Yellowstone national park, *Phys. Geogr.* 29 (2013) 158–178.
- [58] China Code for Design of Photovoltaic Power Station, 2012.
- [59] A.K. Berwal, S. Kumar, N. Kumari, V. Kumar, A. Haleem, Design and analysis of rooftop grid tied 50 kW capacity Solar Photovoltaic (SPV) power plant, *Renew. Sustain. Energy Rev.* 77 (2017) 1288–1299.
- [60] Lingfei Qi, Mingkun Jiang, Yuexia Lv, Jinyue Yan, A celestial motion-based solar photovoltaics installed on a cooling tower, *Energy Convers. Manag.* 216 (2020) 112957.